Lithium Batteries

High-Voltage Pyrophosphate Cathode: Insights into Local Structure and Lithium-Diffusion Pathways**

John M. Clark, Shin-ichi Nishimura, Atsuo Yamada, and M. Saiful Islam

Rechargeable lithium batteries have helped power the consumer revolution in portable electronic devices. The search for alternative cathode materials to replace layered $LiCoO_2$, because of cost and safety issues, has generated considerable research activity,[1–3] particularly for large-scale applications (such as hybrid and pure electric vehicles). An avenue that has been investigated involves the combination of low-cost and abundant iron and phosphate groups (PO_4^{3-}). Owing to the strong binding of the oxygen in the polyanion groups, these materials are more stable and safer than layered transition-metal oxides. To date, most interest has focused on the olivine-structured $LiFePO_4$,[1,4] which has been studied extensively. Other polyanion-type compounds based on silicates,[5] borates,[6] fluorosulfates,[7] and fluorophosphates[8] have also received attention as alternative cathodes.

Recently, it has been proposed that the pyrophosphate $Li_2FeP_2O_7$[9–11] and related compounds[12,13] may provide a new platform for important electrode research. The previously known composition $LiFeP_2O_7$ was found to have significant drawbacks which prevented it from being considered for cathode use.[4,14] In comparison, $Li_2FeP_2O_7$ is easy to synthesize by a conventional solid-state reaction and displays reversible electrode operation at 3.5 V vs. Li/Li^+ without nanosizing or carbon coating.[9] This voltage is the highest for the known Fe-based phosphate cathodes. Although the capacity of $Li_2FeP_2O_7$ is limited to a one-electron theoretical value of approximately 110 mA h g^{-1}, the chemical composition $Li_{2-x}MP_2O_7$ allows for the possibility of a two-electron reaction where the theoretical capacity could reach 220 mA h g^{-1}.

However, the fundamental basis for the performance of this new pyrophosphate is poorly understood, preventing further optimization. To understand the factors influencing the electrochemical behavior of $Li_2FeP_2O_7$ it is clear that more information on the crystal structure and underlying defect and transport properties is needed on the atomic scale.

In particular, there has been little attempt so far to elucidate the diffusion pathways or activation energies that govern Li^+ transport within the pyrophosphate structure, which are important factors for charge/discharge rates and high power.

Herein we use advanced simulation and neutron diffraction techniques to investigate these important issues. The structure of the pyrophosphate is complex and was investigated previously using synchrotron X-ray diffraction.[9] Here, we revisit the structural refinement using an advanced high-power neutron source to determine more accurate structural data of stoichiometric $Li_2FeP_2O_7$ in combination with atomistic modeling of intrinsic defects, dopant incorporation, and Li^+ migration.

First, the crystal structure of stoichiometric $Li_2FeP_2O_7$ was refined with neutron diffraction data obtained from a time-of-flight (TOF)-type diffractometer (Figure 1a). Additional X-ray diffraction data can be found in Figure S1 in the Supporting Information. All the atomic positions in
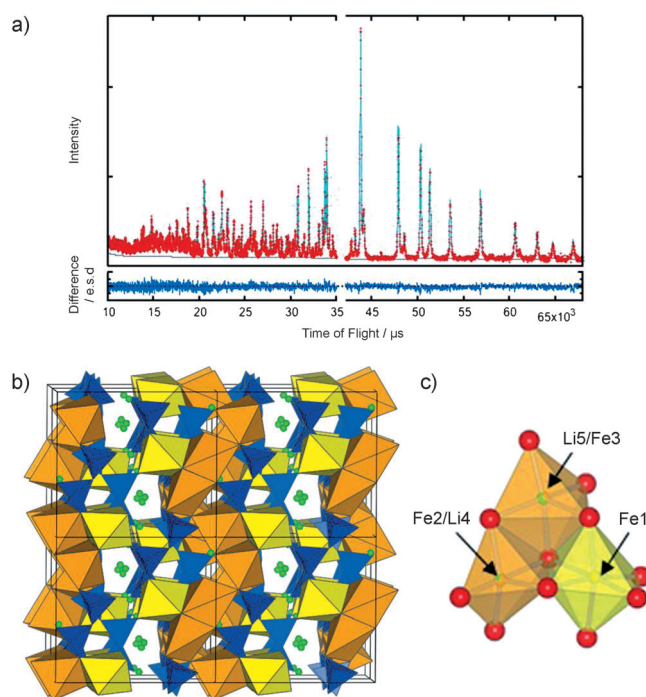
[*] J. M. Clark, Prof. M. S. Islam
Department of Chemistry, University of Bath
Bath, BA2 7AY (UK)
E-mail: m.s.islam@bath.ac.uk

Dr. S. Nishimura, Prof. A. Yamada
Department of Chemical System Engineering
School of Engineering, University of Tokyo
7-3-1 Hongo, Bunkyo-ku, Tokyo 113-8656 (Japan)

Figure 1. a) Rietveld refinement pattern of neutron diffraction data for $Li_2FeP_2O_7$. Red plots, cyan, gray, and blue lines show observed intensity, calculated intensity, background, and residual difference, respectively. b) Crystal structure of $Li_2FeP_2O_7$ showing Li ions (green), FeO_6 ocathedra (yellow), mixed-occupancy FeO_5/LiO_5 units (orange), and P_2O_7 pyrophosphate (blue). c) Close-up view of edge-sharing between an FeO_6 octahedron (fully occupied Fe1 site) and FeO_5/LiO_5 polyhedra (mixed-occupied Fe2/Li4 and Li5/Fe3 sites).

WILEY ONLINE LIBRARY

1

These are not the final page numbers!

$Li_2FeP_2O_7$, including the positions of lithium ions and some structural disorder, were successfully refined. The refined parameters are summarized in Table 1 and Table S1. As in the

Table 1: Lattice constants and experimental data from the neutron diffraction study of $Li_2FeP_2O_7$; a full list of atomic coordinates is given in Table S1 in the Supporting Information.

Parameter	Value	Parameter	Value
M_r	243.67	a [Å]	11.01698(7)
crystal system	monoclinic	b [Å]	9.75416(6)
space group	$P2_1/c$	c [Å]	9.80462(6)
temperature [K]	293	β [°]	101.5444(6)

structural study of a lithium-deficient composition ($Li_{1.75}FeP_2O_7$) that used synchotron X-ray diffraction,[9] the current neutron-diffraction-based refinement shows that $Li_2FeP_2O_7$ is essentially isostructural (space group $P2_1/c$) with $Li_2MnP_2O_7$[15] and composed of $[P_2O_7]^{4-}$ anions which are corner-sharing dimers of PO_4 tetrahedra. Each of the polyhedral units share their corners or edges to form a three-dimensional framework structure (Figure 1 b). The difference between the structures is the existence of significant static disordering among the Li and Fe sites. Li atoms occupy five crystallographic sites and form distorted LiO_4 tetrahedra or distorted LiO_5 trigonal-bipyramids. Fe atoms occupy three sites as FeO_6 octahedra or distorted FeO_5 trigonal-bipyramids. Two of the Li sites and two of the Fe sites are crystallographically identical giving rise to a structure with both Li and Fe mixed occupancies (Figure 1 c); these sites are labeled Li4/Fe2 and Li5/Fe3 and have occupancies of approximately 1:2 and 2:1, respectively (Table S1). We stress that modeling such mixed occupancies with a supercell approach has been important in reproducing the experimental structure of stoichiometric $Li_2FeP_2O_7$.
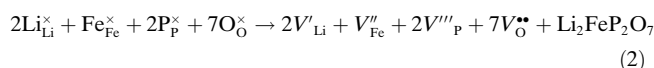
The starting point of the modeling study was reproducing the observed crystal structure. A comparison between the calculated unit cell parameters based on effective potentials (Table S2) and those of the experimental structure are given in Tables S3 and S4. The calculated unit cell parameters deviate from the experimental by at most 1.63 %, and in most cases by much less; the same is found for the Li−O, Fe−O, and P−O bond lengths with mean deviations for the fully occupied sites of less than 0.07, 0.04, and 0.05 Å, respectively. The simulated structure is also in good accord with the diffraction study of $Li_{2-x}FeP_2O_7$ by Kim et al.[10] This reproduction of the relatively complex monoclinic structure gives us confidence that the interatomic potential model can be used reliably in subsequent defect, dopant, and migration calculations. This work extends our previous simulation studies of the $LiMPO_4$ (M = Mn, Fe, Co, Ni) materials[16] and other lithium-battery electrodes (such as Li_2MSiO_4 (M = Mn, Fe), Li_2FeSO_4F, and $LiVO_2$).[17]

A series of isolated point defect (vacancy and interstitial) energies were calculated for the $Li_2FeP_2O_7$ system. These energies were then combined to determine the relative energies of formation of Frenkel- (interstitial) and Schottky-type (vacancy) defects. Examples of these take the following

general forms (using Kröger–Vink notation where V'_{Li} and $Li_i^{\bullet}$ indicate vacancy and interstitial defects respectively):

Li Frenkel [Eq. (1)]:

$$Li_{Li}^{\times} \rightarrow V'_{Li} + Li_i^{\bullet} \tag{1}$$

Full Schottky [Eq. (2)]:

$$2Li_{Li}^{\times} + Fe_{Fe}^{\times} + 2P_P^{\times} + 7O_O^{\times} \rightarrow 2V'_{Li} + V''_{Fe} + 2V'''_P + 7V_O^{\bullet\bullet} + Li_2FeP_2O_7 \tag{2}$$

We also examined the Li/Fe "anti-site" pair defect, which involves the exchange of a Li^+ ion (radius 0.74 Å) with an Fe^{2+} ion (radius 0.78 Å), according to Equation (3).

$$Li_{Li}^{\times} + Fe_{Fe}^{\times} \rightarrow Li'_{Fe} + Fe_{Li}^{\bullet} \tag{3}$$

This type of defect is worth investigating since anti-site or cation-exchange effects have been observed in other polyanionic systems including $LiFePO_4$[16] and Li_2MnSiO_4.[17] It should be noted that two types of Li/Fe anti-site pair defects were considered: one involving the exchange of Li and Fe ions between fully occupied sites (Li1, Li2, Li3, Fe1), and the other involving exchange of ions between mixed-occupied sites (Li4/Fe2 and Li5/Fe3).

Examination of the defect formation results listed in Table 2 reveals three main points. First, the magnitude of the energies suggests that formation of Fe Frenkel, O Frenkel, and Schottky defects is unfavorable. In particular, O^{2-} vacancies and interstitials are highly unfavorable, and unlikely to occur in any significant concentration in the undoped material, confirming the structural stability of the pyrophosphate framework.

Table 2: Energies of Intrinsic Atomic Defects in $Li_2FeP_2O_7$.

Disorder type	Energy [eV]	Disorder type	Energy [eV]
Li Frenkel	1.21	Full Schottky	32.42
Fe Frenkel	3.39	Li/Fe anti-site (Li1, Li2, Li3, Fe1)	0.91
O Frenkel	3.99	Li/Fe anti-site (Li4/Fe2, Li5/Fe3)	0.22

Second, the most favorable type of intrinsic defect for $Li_2FeP_2O_7$ is found to be the Li/Fe anti-site pair as was predicted in an earlier study of $LiFePO_4$.[16] This prediction of anti-site defects in $LiFePO_4$ was confirmed by structural analysis of hydrothermally synthesized $LiFePO_4$,[18,19] and scanning transmission electron microscopy (STEM) studies.[19] The results here suggest that presence of anti-site disorder on mixed-occupied sites is likely to be much more prevalent than on fully occupied sites. The concentration of anti-site disorder would be temperature dependent and hence sensitive to experimental synthesis conditions. Lastly, the second lowest energy defect found for $Li_2FeP_2O_7$ is the Li Frenkel (Table 2), which suggests that a very minor population of this Li vacancy and Li interstitial defects could be present at high temperatures.

We note that intrinsic redox processes such as oxidation and reduction were also considered. In general, the high

energies (> 3.2 eV) suggest that oxidation (with formation of Fe^{3+}) and reduction (with formation of Fe^+) is unlikely to be significant, and are consistent with $Li_2FeP_2O_7$ not exhibiting high intrinsic electronic conduction.

Examination of the Li^+ mobility and pathways in $Li_2FeP_2O_7$ are of vital importance when considering its charge/discharge rates. However, obtaining such insights for complex polyhedral structures is far from straightforward. Simulation methods can greatly enhance our understanding of the migration pathway by evaluating the activation energies for various possible mechanisms at the atomic level.

Figure 2 shows that the Li-diffusion pathways considered involve conventional vacancy hopping between all neighboring Li positions along each of the three principal axes. Energy
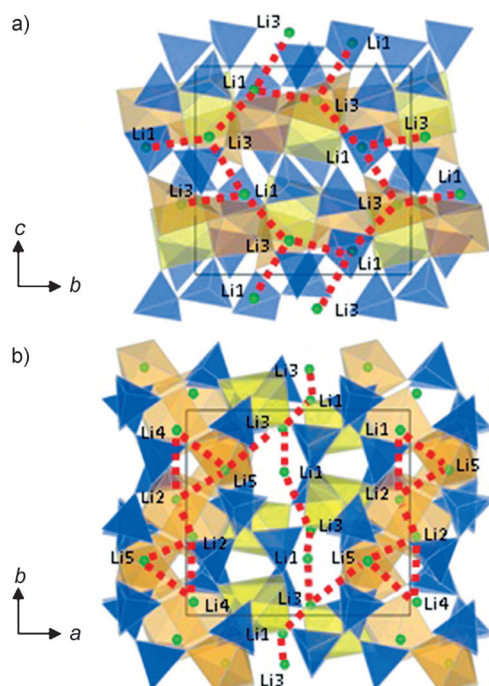
Figure 2. Li^+ migration in $Li_2FeP_2O_7$ with dashed lines showing the diffusion paths considered: a) Li–Li connections parallel to the *b*- and *c*-axes; b) Li–Li connections parallel to the *a*- and *b*-axes.

profiles for Li migration along each of these paths can be mapped out. In this way the position of highest potential energy (i.e., the "saddle-point" configuration) can be identified from which the migration energy is derived; such an approach has been used in numerous studies on oxide ion and cation migration in complex oxides.[16,20] The resulting lowest migration energies for Li diffusion along the three main directions are reported in Table 3.

The lowest energy pathways are found to involve Li diffusion parallel to the *b*- and *c*-axes with energy barriers of 0.40 eV. The final calculated paths for long-range Li^+ diffusion are shown in Figure 3. These paths involve Li1 and Li3 ions which have small separations (2.96–3.19 Å) but, more importantly, the channel that exists in the *bc*-plane is relatively unhindered (Figure 3b). A higher activation energy barrier of 0.73 eV is calculated for migration parallel

Table 3: Calculated Li^+ migration energies and Li–Li distances (for paths shown in Figure 2).

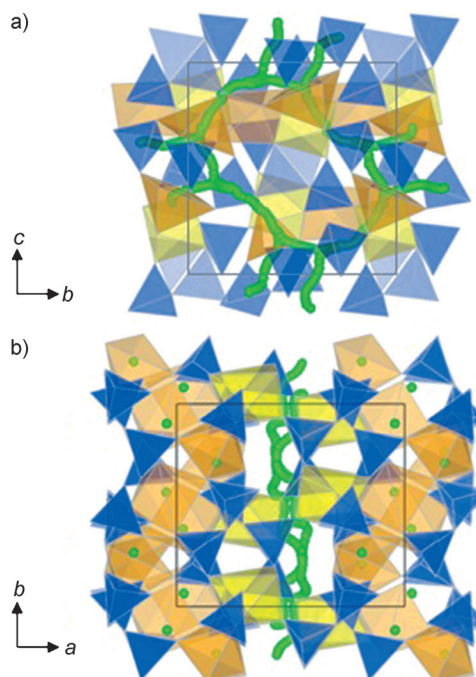| Net diffusion direction	Li ions involved	Smallest separation [Å]	Largest separation [Å]	E_{mig} [eV]
a-axis	Li1,Li2,Li3,Li4,Li5	2.96	3.82	0.73
b-axis	Li1,Li3	2.96	3.19	0.40
c-axis	Li1,Li3	2.96	3.19	0.40

Figure 3. Calculated paths for long-range Li^+ migration involving Li1 and Li3 sites along the *b*-axis and *c*-axis directions with activation energies of 0.40 eV; simulations indicate quasi-2D transport and nonlinear pathways; a) view of the *bc*-plane, b) view of the *ab*-plane.

to the *a*-axis, which involves larger Li–Li separations of up to 3.82 Å and a path that is significantly more hindered by Fe/O and P/O polyhedra. These results indicate high Li^+ mobility within the *b*-axis and *c*-axis channels, and as such $Li_2FeP_2O_7$ shows quasi-two-dimensional (2D) Li migration in the *bc*-plane. This behavior contrasts with that in $LiFePO_4$ which only allows Li^+ migration along 1D channels parallel to the *b*-axis.[16,21]

It is often assumed that the migrating ion takes the shortest path between adjacent sites, that is, a direct linear jump. However, our simulations reveal curved paths between adjacent Li sites (Figure 3), which produces "wavelike" trajectories for long-range migration. It is worth noting that analogous, curved Li^+ migration paths were first predicted from atomistic simulation studies[16] of $LiFePO_4$ which were subsequently confirmed by neutron diffraction maximum entropy method (MEM) analysis.[21] Indeed, one of the aims of the present study is to stimulate similar experimental work on $Li_2FeP_2O_7$ to probe actual Li^+ migration pathways. We recall that the defect calculations suggest that the Li/Fe anti-

site will be much more prevalent for the mixed-occupied sites (Li4/Fe2 and Li5/Fe3) and so will not affect the favorable 2D migration paths involving Li1 and Li3 sites shown in Figure 3.

Although there are no Li$^+$ conductivity data for direct comparison, our calculated Li migration energies are consistent with activation energies for olivine phosphates from dc conductivity and impedance spectroscopy measurements,[22] and are also compatible with experimental activation energies for Li ion conductivity in other framework-structured phosphate materials.[23] Recent theoretical calculations by Adams[24] have provided similar insight into lithium migration paths in related polyanion compounds.

Given that the current operating voltage for Li$_2$FeP$_2$O$_7$ of 3.5 V vs. Li/Li$^+$ was recorded without any technical effort such as nanosizing or carbon coating, it is of interest to investigate the effect of cation doping in order to gauge whether it is likely to result in improved electronic conductivity. Our simulation methods, as used previously to investigate dopant substitution energetics within LiMPO$_4$ (M = Mn, Fe, Co, Ni)[16] can probe these issues for Li$_2$FeP$_2$O$_7$ by generating relative energies of dopant substitution. This approach can provide a useful systematic guide to the site-selectivity for different dopant species and to trends in dopant solubility. In this study we have examined a wider range of dopants in Li$_2$FeP$_2$O$_7$ than experimental reports, from monovalent to pentavalent.

For isovalent dopants (such as Na$^+$ on Li$^+$ or Mg^{2+} on Fe^{2+}), no charge-compensating defect is required. However, for aliovalent dopants (whether donor ions such as Mg^{2+} on Li$^+$ or Al^{3+} on Fe^{2+}, or acceptor ions such as Na$^+$ on Fe^{2+}), the type of charge-compensating mechanism has not been clearly established from experiment, and could consist of either Li vacancies, Fe vacancies, O vacancies, or electronic species (e.g., Fe$^+$, Fe^{3+}). We therefore calculated the overall substitution energy for a variety of different compensation mechanisms described in Supporting Information together with the dopant potentials (Table S5). Dopant incorporation ("solution") energies for a range of cation dopants are plotted as a function of ionic radius in Figure 4.
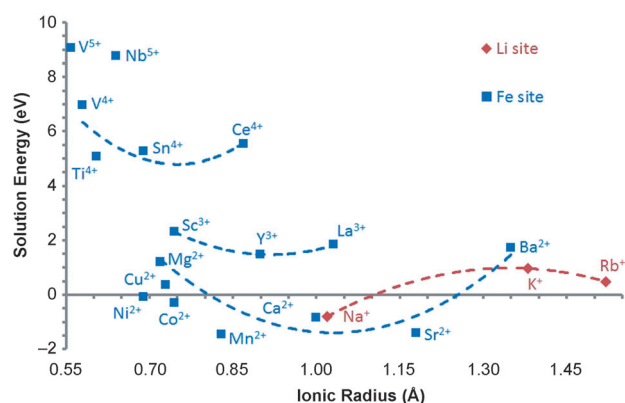

Figure 4. Calculated dopant solution energies versus dopant ionic radius for Li$_2$FeP$_2$O$_7$. Only the most favorable energies for the Li and Fe sites are shown. Lines for M$^+$, M^{2+} (alkaline-earth), M^{3+}, and M^{4+} dopants are guides for the eye.

These results indicate two main features. First, the lowest energies were found for isovalent substitution; in particular, Na$^+$ doping for Li$^+$ and divalent doping (e.g. Mn^{2+}, Ni^{2+}, and Sr^{2+}) for Fe^{2+} were found to be favorable. In general, the less favorable dopant sites were more than 2 eV higher in energy. However, isovalent substitution does not require charge compensation and hence would not lead to an increase in the number of electronic charge carriers.

Partial substitution of Fe by other divalent transition-metal ions may be used to tune (or increase) the Fe^{2+}/Fe^{3+} redox potential through the inductive effect.[2] Interestingly, our results suggest that the most favorable dopant for Fe^{2+} is Mn^{2+}. Indeed, Furuta et al.[12] have recently investigated the Li$_{2-x}$(Fe$_{1-y}$Mn$_y$)P$_2$O$_7$ solid solution and found evidence of enhanced redox potentials approaching 4.0 V.

Second, a key result is that supervalent doping (especially of Nb^{5+} and V^{5+}) is unfavorable. This result suggests that these ions are unlikely to be incorporated above very low concentrations (<3%). The compensation mechanism for such supervalent dopants was found to be Fe^{2+} vacancies, whereas compensation by a change in Fe^{2+} charge state (i.e., to give an Fe$^+$ small polaron species) was much higher in energy. These results suggest that such donor dopants will not lead to changes in Fe oxidation state or to an enhanced electronic conductivity. The overall trends reveal that the greater the difference between the charges of the dopant and host ion, the higher the dopant incorporation energy (e.g., for the Fe site, solution energies increase in the series Co^{2+} < Sc^{3+} < Sn^{4+} < Nb^{5+}). This trend suggests that electrostatic interactions dominate the energetics of dopant incorporation in Li$_2$FeP$_2$O$_7$.

In conclusion, this systematic survey of the Li$_2$FeP$_2$O$_7$ cathode material used a combination of neutron diffraction and atomistic simulation techniques to provide insights into the crystal structure, defect chemistry, and Li$^+$ migration pathways, which can be summarized as follows:

1) The monoclinic structure of stoichiometric Li$_2$FeP$_2$O$_7$ has been elucidated and found to have significant static disordering of the Li and Fe sites. The simulations suggest that the most favorable intrinsic defect is the Li/Fe antisite, especially for the mixed-occupied sites (Li4/Fe2 and Li5/Fe3), which would be sensitive to synthesis conditions.

2) Lithium diffusion will follow nonlinear, curved paths parallel to the *b*- and *c*-axes via Li1/Li3 sites, which show low migration energies (0.40 eV). Hence, in contrast to 1D diffusion in LiFePO$_4$, fast Li$^+$ transport in Li$_2$FeP$_2$O$_7$ is predicted to be through a 2D network in the *bc*-plane, which is important for good rate capability and for the function of particles without nanosizing. The results suggest that synthetic approaches to minimize Li/Fe mixed-occupied sites would enhance the diffusion pathways.

3) Favorable doping is found for Na$^+$ on the Li$^+$ site, and isovalent dopants (e.g., Mn^{2+}, Co^{2+}, Cu^{2+}) on the Fe^{2+} site; the latter could be used in attempts to increase the Fe^{2+}/Fe^{3+} redox potential towards 4 V. In contrast, supervalent doping (especially V^{5+} and Nb^{5+}) appears unfavorable on both Li$^+$ and Fe^{2+} sites; the charge-compensation mech-

↖↖ These are not the final page numbers!

anism found for such doping does not alter the Fe^{2+} valence state and hence is unlikely to enhance electronic conductivity.

The results presented here provide a valuable framework for the future optimization of high-voltage pyrophosphate materials for next-generation lithium batteries.

Experimental Section

Experiments. $Li_2FeP_2O_7$ samples were prepared by conventional solid-state synthesis using stoichiometric amounts of Li_2CO_3 (Wako, 99 + %), $FeC_2O_4 \cdot 2H_2O$ (JUNSEI, 99 + %), and $(NH_4)_2HPO_4$ (Wako, 99 + %). Precursors were thoroughly mixed by planetary ball-milling for 6 h (400 rpm). Cr-hardened stainless-steel milling media and containers were used. The precursor mixture was calcined at 600 °C for 12 h inside a tube furnace with steady argon flow. Upon cooling the mixture to ambient temperature, we obtained the desired $Li_2FeP_2O_7$ powder. Neutron powder-diffraction patterns were taken using the high-throughput diffractometer iMATERIA installed at the megawatt-class pulsed-spallation neutron sources J-SNS at the Japanese particle accelerator research complex (J-PARC). Rietveld refinement was performed using the program Topas-Academic Version 4.1.

Simulations. The atomistic modeling techniques are well-established and detailed elsewhere.[25] The interatomic interactions are treated by effective shell-model Buckingham potentials (Table S2). The transferability of this approach has proved successful in the modeling of structural, defect, and ion-transport properties of a range of lithium-battery and fuel-cell materials.[16,17,26] An important feature of the methods is the treatment of full lattice relaxation of a large number of ions (>1000) around the migrating lithium ion, which is modeled by the Mott–Littleton method (embodied in the GULP code[27]). VESTA[28] was used for analysis of results.

Note added in proof: We have become aware of a very recently published study[29] that also deals with atomistic simulations of lithium migration in transition-metal pyrophosphates.

[1] M. Armand, J. M. Tarascon, *Nature* **2008**, *451*, 652.
[2] J. B. Goodenough, Y. Kim, *Chem. Mater.* **2010**, *22*, 587.
[3] a) B. L. Ellis, K. T. Lee, L. F. Nazar, *Chem. Mater.* **2010**, *22*, 691; b) M. R. Palacín, *Chem. Soc. Rev.* **2009**, *38*, 2565.
[4] A. K. Padhi, K. S. Nanjundaswamy, J. B. Goodenough, *J. Electrochem. Soc.* **1997**, *144*, 1188.
[5] a) A. Nytén, A. Abouimrane, M. Armand, T. Gustafsson, J. O. Thomas, *Electrochem. Commun.* **2005**, *7*, 156; b) M. S. Islam, R. Dominko, C. Masquelier, C. Sirisopanaporn, A. R. Armstrong, P. G. Bruce, *J. Mater. Chem.* **2011**, *21*, 9811.
[6] A. Yamada, N. Iwane, Y. Harada, S. Nishimura, Y. Koyama, I. Tanaka, *Adv. Mater.* **2010**, *22*, 3583.
[7] N. Recham, J. N. Chotard, L. Dupont, C. Delacourt, W. Walker, M. Armand, J. M. Tarascon, *Nat. Mater.* **2010**, *9*, 68.
[8] B. L. Ellis, W. R. M. Makahnouk, Y. Makimura, K. Toghill, L. F. Nazar, *Nat. Mater.* **2007**, *6*, 749.
[9] S. Nishimura, M. Nakamura, R. Natsui, A. Yamada, *J. Am. Chem. Soc.* **2010**, *132*, 13596.
[10] H. Kim, S. Lee, Y. U. Park, J. Kim, S. Jeon, K. Kang, *Chem. Mater.* **2011**, *23*, 3930.
[11] P. Barpanda, T. Ye, S. Chung, Y. Yamada, S. Nishimura, A. Yamada, *J. Mater. Chem.* **2012**, *22*, 13455.
[12] N. Furuta, S. Nishimura, P. Barpanda, A. Yamada, *Chem. Mater.* **2012**, *24*, 1055.
[13] a) A. Jain, G. Hautier, C. Moore, B. Kang, J. Lee, H. L. Chen, N. Twu, G. Ceder, *J. Electrochem. Soc.* **2012**, *159*, A622; b) H. Zhou, S. Upreti, N. A. Chernova, G. Hautier, G. Ceder, M. S. Whittingham, *Chem. Mater.* **2011**, *23*, 293; c) H. Zhou, S. Upreti, N. A. Chernova, M. S. Whittingham, *Acta Crystallogr. Sect. E* **2011**, *67*, 158.
[14] a) A. A. Salah, P. Jozwiak, J. Garbarczyk, K. Benkhouja, K. Zaghib, F. Gendron, C. M. Julien, *J. Power Sources* **2005**, *140*, 370; b) C. Wurm, M. Morcrette, G. Rousse, L. Dupont, C. Masquelier, *Chem. Mater.* **2002**, *14*, 2701; c) J. Kim, D. S. Middlemiss, N. A. Chernova, B. Y. X. Zhu, C. Masquelier, C. P. Grey, *J. Am. Chem. Soc.* **2010**, *132*, 16825.
[15] L. Adam, A. Guesdon, B. Raveau, *J. Solid State Chem.* **2008**, *181*, 3110.
[16] a) M. S. Islam, D. J. Driscoll, C. A. J. Fisher, P. R. Slater, *Chem. Mater.* **2005**, *17*, 5085; b) C. A. J. Fisher, V. M. H. Prieto, M. S. Islam, *Chem. Mater.* **2008**, *20*, 5907.
[17] a) N. Kuganathan, M. S. Islam, *Chem. Mater.* **2009**, *21*, 5196; b) A. R. Armstrong, N. Kuganathan, M. S. Islam, P. G. Bruce, *J. Am. Chem. Soc.* **2011**, *133*, 13031; c) R. Tripathi, G. R. Gardiner, M. S. Islam, L. F. Nazar, *Chem. Mater.* **2011**, *23*, 2278; d) A. R. Armstrong, C. Lyness, P. M. Panchmatia, M. S. Islam, P. G. Bruce, *Nat. Mater.* **2011**, *10*, 223.
[18] J. J. Chen, M. J. Vacchio, S. J. Wang, N. Chernova, P. Y. Zavalij, M. S. Whittingham, *Solid State Ionics* **2008**, *178*, 1676.
[19] S. Y. Chung, S. Y. Choi, T. Yamamoto, Y. Ikuhara, *Phys. Rev. Lett.* **2008**, *100*, 125502.
[20] M. S. Islam, P. R. Slater, *MRS Bull.* **2009**, *34*, 935.
[21] S. Nishimura, G. Kobayashi, K. Ohoyama, R. Kanno, M. Yashima, A. Yamada, *Nat. Mater.* **2008**, *7*, 707.
[22] a) C. Delacourt, L. Laffont, R. Bouchet, C. Wurm, J. B. Leriche, M. Morcrette, J. M. Tarascon, C. Masquelier, *J. Electrochem. Soc.* **2005**, *152*, A913; b) J. Y. Li, W. L. Yao, S. Martin, D. Vaknin, *Solid State Ionics* **2008**, *179*, 2016.
[23] L. Sebastian, J. Gopalakrishnan, *J. Mater. Chem.* **2003**, *13*, 433.
[24] S. Adams, R. P. Rao, *J. Mater. Chem.* **2012**, *22*, 1426.
[25] C. R. A. Catlow, *Computer Modelling in Inorganic Crystallography*, Academic Press, San Diego, **1997**.
[26] a) P. M. Panchmatia, A. Orera, G. J. Rees, M. E. Smith, J. V. Hanna, P. R. Slater, M. S. Islam, *Angew. Chem.* **2011**, *123*, 9500; *Angew. Chem. Int. Ed.* **2011**, *50*, 9328; b) E. Kendrick, M. S. Islam, P. R. Slater, *Chem. Commun.* **2008**, 715.
[27] J. D. Gale, A. L. Rohl, *Mol. Simul.* **2003**, *29*, 291.
[28] K. Momma, F. Izumi, *J. Appl. Crystallogr.* **2008**, *41*, 653.
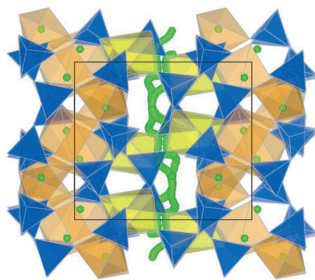[29] S. Lee, S. S. Park, *Chem. Mater.* **2012**, *24*, 3550.

Communications

Lithium Batteries

J. M. Clark, S. Nishimura, A. Yamada,
M. S. Islam* ———————— ▮▮▮▮–▮▮▮▮

High-Voltage Pyrophosphate Cathode:
Insights into Local Structure and Lithium-
Diffusion Pathways

Ion-transport paths: Combined modeling and neutron diffraction studies provide atomic-scale insights into $Li_2FeP_2O_7$, a material proposed for a new lithium-battery cathode with reversible electrode operation at the highest voltage of all known Fe-based phosphates. The results indicate that Li^+ ions are transported rapidly through a 2D network along the paths shown in green in the picture.